X-33 Attitude Control System Design
for
Ascent, Transition, and Entry Flight Regimes

IN -08
375 988
Ⓒ W/ Hive D

Charles E. Hall[++], Michael W. Gallaher[++], Neal D. Hendrix[+]

NASA Marshall Space Flight Center

Huntsville, Alabama, 35812

Abstract

The Vehicle Control Systems Team at Marshall Space Flight Center, Systems Dynamics Laboratory, Guidance and Control Systems Division is designing, under a cooperative agreement with Lockheed Martin Skunkworks, the Ascent, Transition, and Entry flight attitude control system for the X-33 experimental vehicle. Ascent flight control begins at liftoff and ends at linear aerospike main engine cutoff (MECO) while Transition and Entry flight control begins at MECO and concludes at the terminal area energy management (TAEM) interface. TAEM occurs at approximately Mach 3.0. This task includes not only the design of the vehicle attitude control systems but also the development of requirements for attitude control system components and subsystems. The X-33 attitude control system design is challenged by a short design cycle, the design environment (Mach 0 to about Mach 15), and the X-33 incremental test philosophy. The X-33 design-to-launch cycle of less than 3 years requires a concurrent design approach while the test philosophy requires design adaptation to vehicle variations that are a function of Mach number and mission profile. The flight attitude control system must deal with the mixing of aerosurfaces, reaction control thrusters, and linear aerospike engine control effectors and handle parasitic effects such as vehicle flexibility and propellant sloshing from the uniquely shaped propellant tanks. The attitude control system design is, as usual, closely linked to many other subsystems and must deal with constraints and requirements from these subsystems.

I. Introduction

The X-33 is comprised of both rocket and aircraft vehicle design and requires analytical methods for evaluating the flight performance that draws from, but is not limited to, each field [7]. The propulsion system design, mission specific trajectory constraints and engine out abort capability are among many of the challenges.

Ascent attitude control is provided by rocket engine thrust vector control (TVC) and aerosurfaces. The vehicle uses two linear aerospike engines with upper and lower banks of thrusters on each engine as depicted in figure 1. Unlike conventional launch vehicles, however, TVC is accomplished by differentially throttling the upper and lower banks of thrusters for pitch and roll, and differentially throttling the left and right engines (both upper and lower banks) for yaw.

[++] Aerospace Engineer, Flight Mechanics, GN&C Systems Branch
[+] Team Leader, Flight Mechanics, GN&C Systems Branch

Eight aerosurfaces are used for ascent and entry control; four elevons, two flaps and two rudders, as shown in figure 2. Inherent to using aerosurfaces are concerns about cross axis control torque coupling and aerodynamic loading on the surfaces.
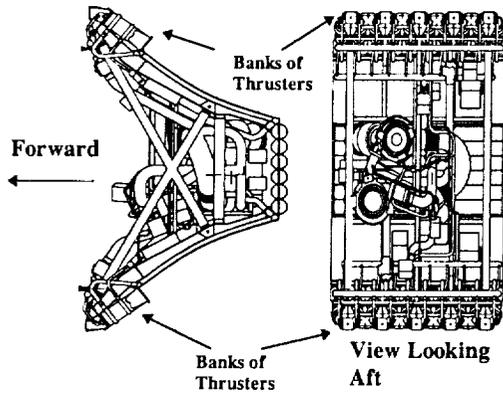
Figure 1: Linear Aerospike Engine.
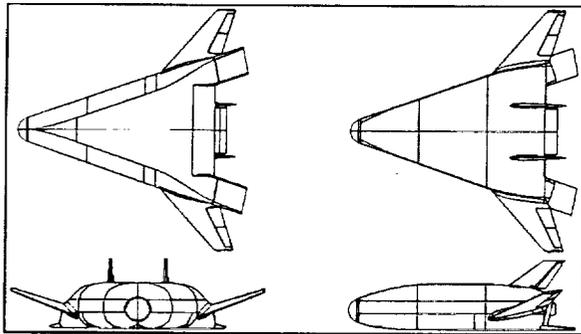
Figure 2: X-33 Aerosurface Configuration.

Due to the shape of the lifting body fuselage, complex tank structures were included in the vehicle design. There are two liquid hydrogen tanks located aft in the vehicle, and one liquid oxygen tank located in the nose. Extensive analysis was required to derive the degree of propellant damping required to provide attitude control stability and stability margins during ascent for all missions.

The control law design was based upon past launch vehicle experience and upon analysis of two other Single Stage To Orbit Reusable Launch Vehicle

concepts [1,2]. Due to the short design cycle and the need for rapid prototyping, a well tested and reliable attitude control system architecture was chosen for the X-33. This design provides excellent ascent trajectory tracking and is robust to wind disturbances and non-linearities such as control effector deadzones and control effector saturation. Concurrent with analyses using the chosen design, research in attitude control with Sliding Modes [9] looks promising, and could find application in the full scale Reusable Launch Vehicle.

Flight control design and analysis required analytical software tailored to time and frequency domain analysis with rapid prototyping in mind. MARSYAS (MARshall SYstem for Aerospace Simulation) [3] was employed for the control system design and development. The MARSYAS simulation system has been under continuous development at Marshall Space Flight Center since the 1960's and has been used for the analysis of a variety of launch vehicles, spacecraft and the Space Shuttle Main Engine. Dynamic modeling can be realized quickly using the MARSYAS simulation language and assembled into a full system simulation very quickly. MARSYAS is capable of time domain and frequency domain 6 Degree-of-Freedom (6DOF) analysis using the same models for both domains.

Although MARSYAS can be used for time domain analysis, it must process the simulation code in a translation phase that converts the simulation code to C, then links to C libraries to form an executable simulation. The equations are arranged to make them amenable to frequency response and eigenvalue analysis. This requires more CPU time making MARSYAS inefficient for large sets of simulations as required for dispersion analysis. For dispersion analyses with higher fidelity models, MAVERIC (Marshall Aerospace VEhicle Representation In C) [4] was used. MAVERIC can be used for 6DOF or 3DOF simulation from lift off to TAEM, and can produce Monte Carlo analysis of both ascent and entry profiles.

II. Reference Mission Profile

The X-33 will launch from Edwards Air Force Base, California and land at one of two sites. A reference flight profile from launch to TAEM is

shown in figure 3. One typical mission's ascent phase of flight lasts 203 seconds and places the vehicle at an altitude of roughly 180,000 feet and a speed of Mach 10. During ascent, variations in engine throttle (100% to 63% nominal power level) and rigorous attitude maneuvers must be accomodated by the control system in order to meet the required MECO conditions on altitude, velocity, angles of attack (α) and side slip (β) before hand-over to transition and entry flight control. Guidance is open nominally loop for ascent, and the attitude control system follows commanded inertial roll, pitch, yaw angles and body rates. After MECO, the transition phase, which lasts approximately 25 seconds, re-configures the control mixing from main engines with aerosurfaces to aerosurfaces with RCS. The attitude control system for the transition and entry phases of flight follow commanded α, α rate, β, bank and bank rate profiles generated by guidance. Guidance is closed loop during the entry phase. The entry phase of flight brings the vehicle from an altitude of approximately 191,000 feet and a speed of Mach 9.8 down to an altitude of 89,000 feet and a speed of Mach 3.0.
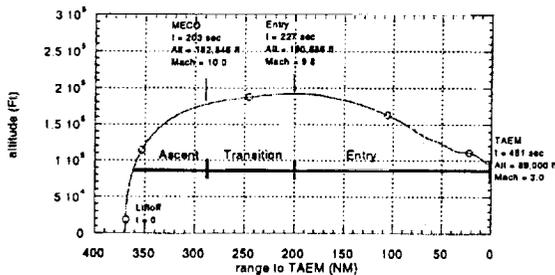
Figure 3: Reference Mission Profile

III. Ascent Flight Control

Control System Description

The function of the Ascent Flight Control System (AFCS) is to provide stable control of the vehicle from liftoff to MECO while following the prescribed ascent trajectory provided by the Guidance function. A block diagram of the AFCS is given in figure 4. The attitude quaternion, body rate, engine throttle and mixture ratio commands are received from Guidance at a 1hz rate. The AFCS functions are executed at a 50 hz rate, which requires smoothing the commands. Gains, limits and flex filter coefficients are pre-computed for each separate mission and loaded

before flight. The AFCS is designed to accommodate an engine failure. It requires no re-configuration to do this; instead, a different set of control gains are used, chosen as a function of the time of failure.
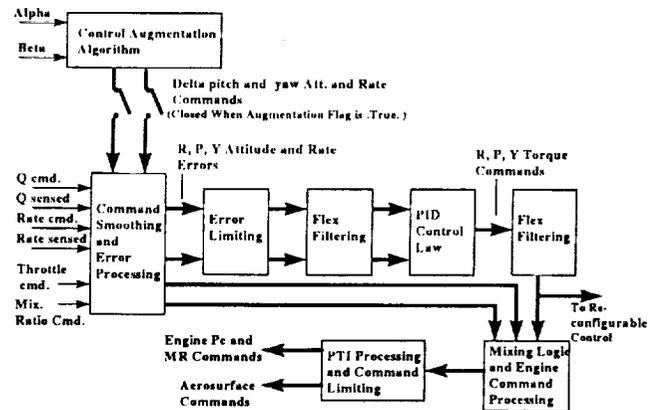
Figure 4: AFCS Block Diagram

In the case of an aerosurface actuator failure, the AFCS computes torque commands using nominal gains, filters them and passes them to a reconfigurable control algorithm that essentially redistributes the control to the remaining operable surfaces, taking advantage of the multi-axis torque capability of each one [8]. An air data control augmentation system is in place for load relief, that uses measured α and β as inputs, and generates augmented pitch and yaw attitude and rate error commands. It is activated by a software flag that is set at a pre-determined time of flight or Mach number. This paper includes only analysis results from the AFCS without air data augmentation, however. The capability to include Programmed Test Inputs (small, temporary open loop commands) was built in so that engine and aerodynamic characteristics could be studied from post flight data.

Control Effectors

The X-33 uses two linear aerospike rocket engines and eight aerosurfaces for attitude control during ascent. The linear aerospike engines, which use liquid oxygen and hydrogen propellants, provide 207,000 pounds thrust each. The design allows the exhausted gasses to expand against the atmosphere, as opposed to a bell shaped nozzle like conventional engines, and is self-compensating with altitude. Each engine has a bank of ten thrusters across the top and bottom which can be throttled independently of one

another. Thrust Vector Control (TVC) is done by differentially throttling each bank of thrusters, so that the need for a gimbal system is eliminated. Furthermore, the engine can be integrated into the thrust structure, stiffening the design and saving weight. Effects of the linear aerospike engines on the aerodynamics of the vehicle and aerodynamic effects on the engine's performance must be accounted for, however. Since this type of engine has never been used on any vehicle, these effects had to be derived through a combination of computational fluid dynamic analysis and wind tunnel testing of an X33 model with a simulated engine. This data will be augmented by data from planned flight tests of a subscale aerospike engine ramp on the SR-71.

Figure 5 illustrates how TVC is accomplished using differential throttling. If no TVC is required, both the top and the bottom banks of thrusters have the same throttle setting. For roll control, one engine's thrusters are commanded differentially to produce a pitch torque, and the other engine is commanded in the same way to produce pitch torque of opposite sign.

a.)   b.)

c.)
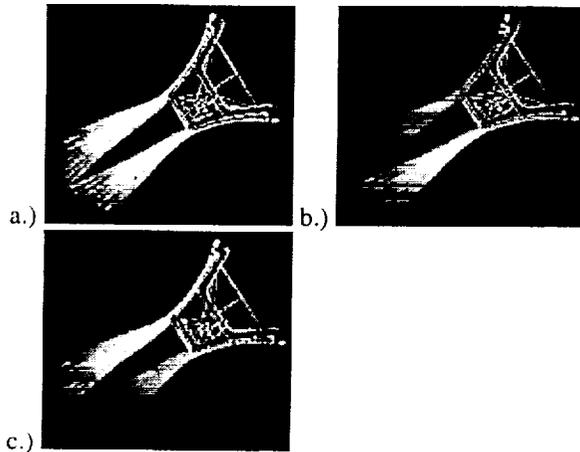
Figure 5: Aerospike Engine; a) No TVC, b) pitch up differential throttle, c) pitch down differential throttle

For pitch control, the differential throttle command is the same for both engines. To produce yaw torque, the overall throttle command for one engine is higher than the other one. In nominal operation, each engine's Gas Generators (GG) are throttled for yaw TVC. The oxygen and hydrogen feed lines from the GG's to the TVC valves are interconnected and can

be opened or closed by isolation valves. These valves are closed under nominal conditions. In the case of an engine failure, they can be opened allowing one GG to provide flow to both engines thus providing TVC operation similar to the nominal, but with reduced thrust.

Figure 2 illustrates the aerosurface configuration. On ascent, the vertical rudders are used for yaw, the elevons and flaps are used for roll and pitch control. There are two elevons on each canted fin, but the AFCS treats them as one surface, sending the same deflection command to both.

Optimal Control Effector Selection Algorithm

An Optimal Control Effector Selection Algorithm [5] was employed to generate the gains used in the mixing logic for the AFCS. A function of control effector deflections is formed:

$$f(\delta) = \delta^T Q \delta \qquad (1)$$

where δ is a 8x1 vector of effector deflections, and Q is a positive symmetric matrix (8x8) of weighting or penalty factors. A constraint equation is written that equates commanded torque (T_c) about the roll, pitch, and yaw axes of the vehicle to the corresponding effector deflections:

$$\Phi(\delta) = D\delta - T_c = 0 \qquad (2)$$

where D, called the sensitivity matrix, is a (3x8) matrix of partial derivatives of torque about roll, pitch, and yaw with respect to each effector deflection. A new functional of the form

$$g(\delta) = f(\delta) + \lambda^T \Phi(\delta) \qquad (3)$$

is written, where λ is the lagrange multiplier and is independent of δ. For a minimum set of deflections δ that satisfy the constraints (2), the equation

$$\frac{\partial\left[g(\delta)\right]}{\partial\delta} = 0 \qquad (4)$$

must be satisfied. Substituting (1) and (2) into (3) and substituting the resultant into (4) yields the following result for δ:

$$\delta = -\frac{1}{2}Q^{-1}D^{T}\lambda \qquad (5)$$

Substituting (5) into (2) and solving for λ yields

$$\lambda = -2\left[DQ^{-1}D^{T}\right]T_{c} \qquad (6)$$

Using LaGrange multipliers and making the appropriate substitutions yields the control deflection vector, δ:

$$\delta = Q^{-1}D^{T}\left[DQ^{-1}D^{T}\right]^{-1}T_{c} \qquad (7)$$

where $B_{v} = Q^{-1}D^{T}\left[DQ^{-1}D^{T}\right]^{-1}$ is the allocation (mixing gain) matrix. Equation (7) yields the deflections that minimize the functional in equation (1) and satisfies the constraint equation (2).

The allocation matrix B_{v} is precomputed at 10 second intervals for each trajectory. Through real wind dispersed simulation analysis, the weighting of each effector is fine-tuned such that each one is used approximately the same percentage.

Flexible Body Dynamics and Flex Filter Design

Flexure in the vehicle structure can be sensed by the rate gyros. Instability can occur when flex modes are excited by the control effectors. Attitude and attitude rates containing flexible body effects are fed back to the attitude control system. For this reason the flexible body dynamics must be accurately modeled and a filter must be designed that attenuates the sensor response to the undesirable modes.

Over 190 modes were identified in the frequency range of interest, 0 to 25 hz, by Finite Element Model analysis. Modes were selected, based on kinetic energy, for various propellant loads. The modes were modeled by a second order differential equation that describes the motion due to flex at the sensor location. The angular rates and displacements due to flex were added to the rigid body rates and displacements. The equation for flex is [6]:

$$\ddot{\eta}_{i} + 2\zeta_{i}\omega_{i}\dot{\eta}_{i} + \omega_{i}^{2}\eta_{i} = \sum_{j=1}^{14}F_{j}$$

Where η_{i}, ζ_{i}, ω_{i}, are the the modal coordinate, generalized damping, and natural frequency of mode i; F_{j} are the generalized forces for mode i at node j. The generalized forces are input to the structure at 14 nodes representing aerosurface actuator and engine hard points. The flex contribution of each mode to the angular velocity measured at the sensor is:

$$\omega_{x,y,z} = \phi_{x,y,z}\dot{\eta}_{i}$$

Where $\phi_{x,y,z}$ is the normalized mode shape at the sensor location.

Filtering the sensor output due to flex modes was accomplished by two digital filters in the Inertial Navigation Unit (INU) and digital notch filters in the AFCS software. The filters in the INU are effectively low pass filters designed to attenuate signals above 10 hz. The AFCS filters were designed to attenuate particular flex modes.

Slosh Dynamics and Damping Requirements

Propellant sloshing is another potential source of instability for the attitude control system. Like flex dynamics, slosh is a parasitic effect that must be modeled in the controls analysis software. Testing was done at Marshall Space Flight Center on sub-scale X-33 tank sections in order to help characterize slosh frequencies in the oxygen and hydrogen tanks. These data, in conjunction with analytical results, were used to define the necessary parameters to model slosh. These parameters, slosh mass, slosh

mass location, and frequency were generated as a function of liquid height in the tanks.

A spring-mass-damper model was used for each slosh mass in the control analysis [10]. Slosh dynamics in the Z body axis or pitch direction, and in the Y body axis or yaw direction for each slosh mass was modeled by second order differential equations, with inputs a function of vehicle accelerations:

$$\ddot{Z}s_i + 2\zeta s_i \omega s_i \dot{Z}s + \omega s_i^2 Zs = f(\ddot{\theta},\ddot{\phi},\ddot{Z}) \quad (8)$$

$$\ddot{Y}s_i + 2\zeta s_i \omega s_i \dot{Y}s + \omega s_i^2 Ys = f(\ddot{\psi},\ddot{\phi},\ddot{Y}) \quad (9)$$

Where ζs_i, ωs_i are the damping coefficient and natural frequency for slosh mode i, $\ddot{\phi},\ddot{\theta},\ddot{\psi}$ are vehicle roll, pitch, and yaw angular accelerations, $\ddot{Z},\ddot{Y}$ are vehicle Z and Y axis accelerations.

Through linear analysis with slosh, damping requirements for the propellant tanks were derived by increasing the damping coefficients in equations (8) and (9) until gain and phase margins in all rotational axes were met. This data was used to design baffles in the oxygen tank. No baffles were needed in the hydrogen tanks because internal septums provided sufficient damping. A plot of the pitch axis damping requirement is shown in figure 6.
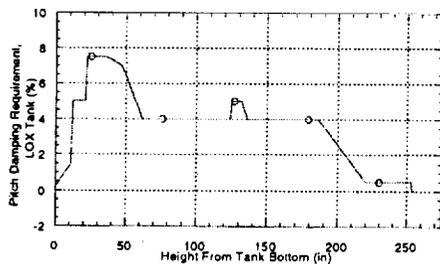
Figure 6: Oxygen tank pitch axis damping requirement

Stability Analysis

Stability of the vehicle was assessed at discrete operating points along the reference ascent trajectory by linear analysis. Nonlinear, time varying models were used to calculate the PID and mixing gains.

Then the frequency responses with slosh and with flex dynamics were computed. The stability margin requirements were 6 db gain and 30 degrees phase for the nominal vehicle. Figure 7a shows a frequency response in the roll channel, opened at the output of the controller, with only smooth wall (0.2%) damping of the liquid oxygen (LOX) slosh modes. The stablity margin boundary is represented by the triangle. A damping of 4% was applied to the LOX slosh modes so that the stability margin requirements could be met. This frequency response in shown in figure 7b.

a.)

b.)
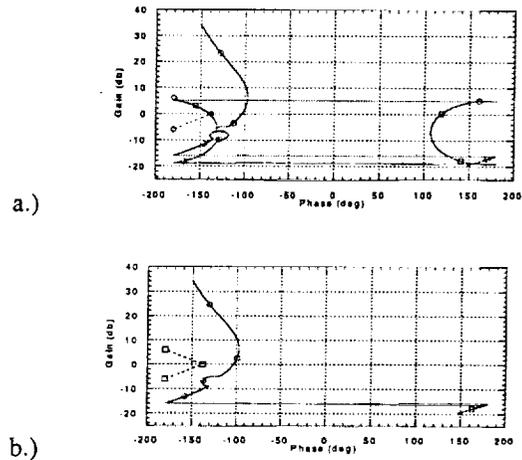
Figure 7: Frequency response with smooth wall damping (a) and 4% damping (b) of slosh modes.

Nonlinear Simulations

Full, nonlinear six degree of freedom simulations of all ascent trajectories were performed to verify the performance of the AFCS for nominal, engine out abort flights, as well as flights with wind and vehicle dispersions. Figure 8 shows attitude errors from over 500 Monte Carlo simulations with wind and vehicle dispersions. The AFCS appears to be robust to these dispersions, ensuring good launch probability.
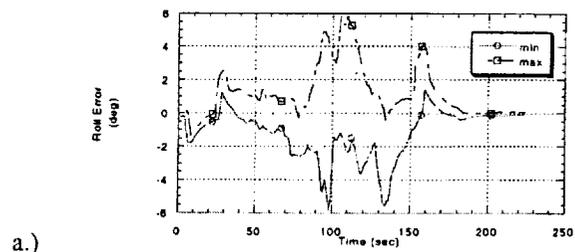
a.)

b.)
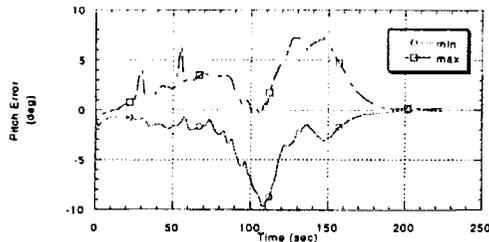
c.)
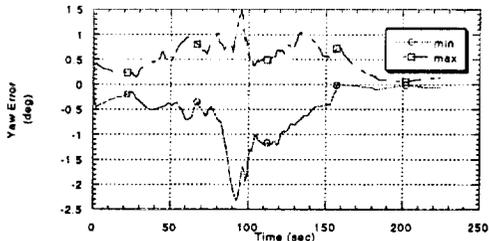
Figure 8: Minimum and maximum attitude errors in (a) roll, (b) pitch and (c) yaw from Monte Carlo simulations.

Figure 9 shows roll, pitch and yaw attitude errors for a trajectory with an engine failure at 100 seconds. The plot demonstrates that the AFCS handles the transition from nominal to engine out flight very well and follows the commanded attitude with good transient response to the maneuvers.
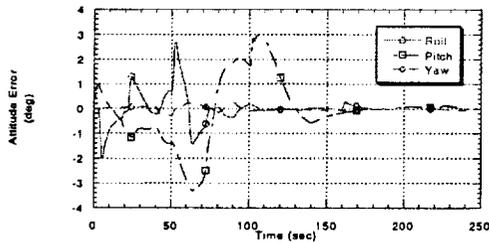
Figure 9: Attitude errors with an engine failure at 100 seconds.

IV. Transition and Entry Control

Transition and Entry Control System Description

The primary responsibility of the X-33 transition and entry flight control system is to generate commands to the control effectors so that the vehicle's attitude and attitude rates follow, to the required degree, the commanded attitude and attitude rates generated by the transition and entry guidances. During transition, the maneuvers initiated by the control system reorient the X-33 from its state at the time of MECO to a state from which guidance can begin to direct the vehicle through the appropriate maneuvers for entry. During entry, the control system initiates maneuvers which are considerably more complex, and which modulate the vehicle's energy, through lift and drag, to reach a targeted velocity, altitude, and location over ground from which the TAEM phase (which is responsible for directing the X-33 to the landing site) can begin.

In order to effect the maneuvering for which it is responsible, the transition and entry control system generates commands to the various control effectors available during these phases: a suite of eight thrusters in the Reaction Control System (RCS) and eight actuated aerosurfaces (two rudders, four elevons, and two body flaps). Due to the difference in computational frequency (guidance commands are updated at 1 Hz, control is executed at 50 Hz) the control system uses a smoothing function to interpolate the commands, reducing the step function effects that can result.

The commands generated by the transition and entry guidances for input to the transition and entry flight control system are expressed in terms of the aerodynamic angles, α, β, and ϕbk (bank angle). The modulation of α affects the balance of lift and drag on the vehicle. β is to be kept to a minimum to minimize loads on the X-33. ϕbk maneuvers and α modulation enable the vehicle control its drag in targeting the desired TAEM conditions. The sign of ϕbk controls lateral motion. Guidance also provides a commanded bank angle rate and angle of attack rate, which the control system uses to incorporate appropriate accelerations. Locally, the control system generates commands for β angle rates; these are typically 0 deg/s, although they may be set to small values with directions selected so that the β control signals will contribute beneficially rather than adversely to a particular commanded bank maneuver.

As the X-33 flies at angles of attack ranging between around 0 to around 50 degrees during transition and entry, bank maneuvers must be

7

accomplished by combinations of roll (about the x-body axis) and yaw (about the z-body axis). Maneuvers about these axes also contribute to β, so the control system's efforts to effect bank must be balanced with its efforts to maintain low β. The commanded β rates can assist in this conflict by forcing the β from an adverse toward a proverse direction.

Complicating the control system's responsibility of controlling to aerodynamic angle commands is the problem of estimating these angles. The relative velocity vector is largely determined by the orientation of the vehicle's velocity vector with respect to the mass of air rotating with the Earth, but winds also contribute to it. The X-33 has no sensors to directly sense these winds and thus measure the aerodynamic angles during most of the transition and entry (a Flush Air Data System is onboard, but is not usable at the higher Mach numbers). Therefore, the navigation system supplies an estimate of α and β computed without consideration of wind. These estimates result in errors that can be significant to the controller, and which must be accommodated with a design that is robust enough to tolerate them.

Figure 9 shows a typical commanded α profile for transition and entry, with the simulated response. Aside from some small perturbations that result from trajectory optimization during design, the commands are slow-changing and relatively non-complex. The disturbances from wind may represent the most significant of any abrupt errors introduced in the pitch axis.
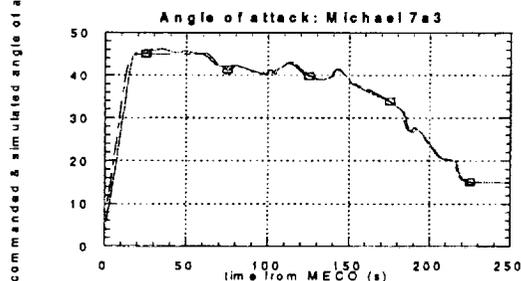
Figure 9: Angle of attack vs. commanded angle of attack.

The β angle is a crucial parameter to control. Due to the navigation errors, this angle can actually be of a

different sign than is estimated in flight. Large β may result in loss of control at higher dynamic pressures, when the base aerodynamic torques can exceed the control authority. While β angles of appropriate sign can assist a commanded bank, it is difficult to maneuver with certainty to a desired β, because the error band is close to the limits to which the controller attempts to constrain β. Early in the design, aerodynamic coefficients dictated that the center of gravity and moment reference point be nearly coincident to provide adequate control authority for angle of attack. This yielded nearly neutral static stability of β. This produces undesirable complications, offset by positive Cn_β dynamic which provides some dynamic stability. But β is routinely disturbed during the bank maneuvers, since bank and β are cross-coupled.

The commanded bank commands are limited in magnitude by guidance. Banks can become very large, and in some cases, overshoot may result in transient periods during which the X-33 is flying banked such that the lift vector is directed downward, but the control system design goals are to avoid such a state. Figure 10 shows a typical bank command profile and simulated response for an early mission.
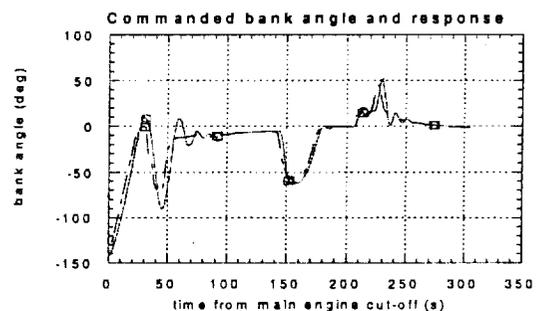
Figure 10: Commanded and simulated bank angle

The missions are designed to more aggressively test various limits of the system, and consequently the commanded profile becomes more challenging for the control system. Figure 11 shows a bank command profile for a later mission. Comparison with the previous figure reveals a greater number of bank reversals and more complex maneuvers.
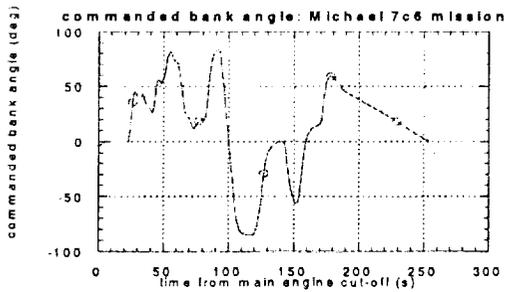
Figure 11: Commanded bank angle, Michael 7c6

Control Effectors: Aerosurfaces and Reaction Control Jets

Figure 2 shows the general locations on the vehicle body of the actuated aerodynamic surfaces used during transition and entry control. The body flaps offer their highest control authority in the pitch axis, and generally exceed the other aerosurfaces in their capacity to generate pitch torque. The elevons are surfaces mounted on the canted fins on either side at the rear of the X-33. The elevons are each split into two surfaces, which are actuated in unison rather than individually. The elevons provide a complex blend of roll, pitch and yaw torque when deflected. The balance between torque varies widely as a function of Mach number and aerodynamic attitude. The rudders are mounted on two side-by-side vertical fins positioned at the top rear of the X-33, centered about the roll axis.

At transition, the dynamic pressure is so low that the rudder effectiveness is inconsequential. During entry, the X-33 is at a large positive α so that the rudders are blocked by the body of the vehicle from most air flow, rendering them impotent. As the α is decreased toward the end of entry, the rudders can provide some useful torque generation capability, but this capability is still far smaller than that provided by the other surfaces.

A major challenge in relying primarily on the aerosurfaces for control during entry is in designing a system robust enough to handle dispersions from predicted effectiveness. As updates to the aerodynamic database have been developed, the strategies have been rethought, and the control system has been structured to allow simple reallocation of the surfaces through mission data loads. This mixing logic, like the gains of the system, are input as a function of Mach number, which, with α, are the primary variables by which effectiveness is predicted. The final configuration of control effectors is a rather highly constrained one. The limited number of aerosurfaces reduces options for redundancy. It is not possible to dedicate each individual aerosurface to a single axis of control (that is, to reserve one set of surfaces for pitch, one for yaw, and one for roll control).

The RCS jet general positions and orientations are shown in Figure 12. These jets provide approximately 500 lbf thrust each in nominal operation. The configuration has been revised as the design proceeded to maximize their usefulness: the downward-thrusting jets on the upper sides are canted so that their firings produce both yaw and roll in directions favorable to banking at the missions' α ranges. However, the RCS system is not capable, in general, of providing pure moments. It may have unpredicted influences on the aerodynamic characteristics of the vehicle and its control surfaces. Some jets fired alone can produce undesirable cross-axis effects. The RCS system has primacy in the control effectiveness strategy during the early part of transition and entry, when the lower dynamic pressure results in decreased effectiveness of the aerosurfaces, but it remains active, to a mission-specifiable degree, well after the aerosurfaces assume primary control. This provides control authority should the aerosurface deflections become saturated or disabled. This phasing of control primacy is achieved through the scheduling of deadbands of the jet selection logic and the mixing logic gains. The RCS allocation strategy is designed to yield a limited amount of redundancy where available, and to meet requirements limiting the number of thrusters that can be commanded on at a given point in time. Violation of these requirements could result in both temporary reductions in effectiveness or permanent thruster failures.

9

yaw/ roll/ pitch down

yaw /roll/ pitch down

yaw

aft facing forward

yaw

yaw/ roll/ pitch up

yaw/ roll/ pitch up

rear from top view

yaw

yaw
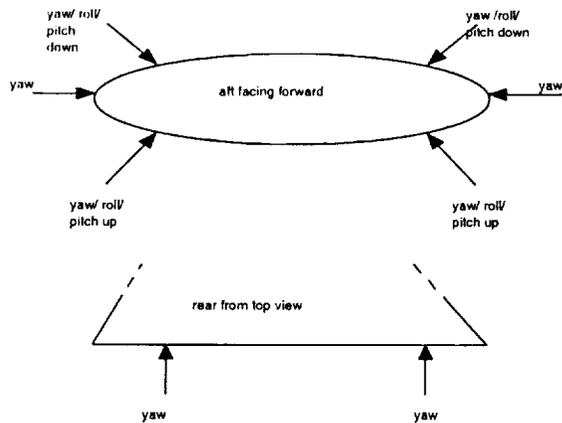
Figure 12: RCS jet locations.

With the aerosurfaces, the primary control allocation strategy is to use the body flaps for control of pitch and yaw. A uniform component of the control signal deflects both body flaps the same amount for pitch, while a smaller differential component is added to one and subtracted from the other, to produce yaw. The elevons are deflected upwards to effect roll. Upwards deflections are expected to produce far less adverse yaw, so that small differential body flap deflections can counter disturbances in that axis. Deflections downwards are permissible for additional pitch control, if the amount of downard deflection is uniform. The control system generates a component of deflection for each aerosurface in response to the commands for torque in each axis, although the factors are zero in many cases. This allows for the revision of control strategy to accommodate updates to the aerodynamic characteristic models that might indicate effectiveness reversals or altered levels of effectiveness.

Ultimately, the available set of control effectors for the X-33 during transition and entry is a fairly tightly-constrained one, and control allocation for nominal and contingency operations is the major challenge of the control system.

Transition and Entry Control Law

Figure 13 shows a simplified block diagram of the first stage of the transition and entry flight control system. Not depicted are certain filters which have been reserved for modifying error signals and some dead zones which can be used to tune responses. The system is essentially a proportional-integral-derivative (PID) style control, using the estimated angle of attack to transform the signals generated by aerodynamic angle and rate errors into body axis torque requests. The command signals are further processed with the mixing logic, which allocates these signals to the control effectors based upon a Mach schedule.

The parameters of the control system are selected initially through a process of linearized stability analysis, performed at several points in a given mission. These parameters are selected to provide acceptable response at representative phases in the flight, covering the range of aerodynamic model points and periods of critical performance. This provides a set of mission data loads corresponding to particular Mach numbers. By examining how these parameters change between Mach, a good idea of what ranges are appropriate and reasonable is obtained, with an estimate of how different elements of the controller must be weighted. The parameters of the control system are tuned through a series of 6 degree-of-freedom simulations, assuring that the performance displays the required response characteristics. Control system robustness is further verified by applying the Monte Carlo technique to the simulation process, exposing the design to as full a range of dispersions in parameters as possible. These dispersions include the mechanical tolerances such as thruster locations, analytic uncertainties such as aerodynamic coefficient ranges, and statistical dispersions generated with the Global Reference Atmosphere Model [11] which simulates perturbed winds and atmospheres.

The dispersion analysis has not yet been completed, but intermediate results have shown increasing robustness. Gain sets developed for one mission have been satisfactorily applied to nominal simulations of another mission, suggesting that the parameter selection methodology is in itself leading to a robust control specification.
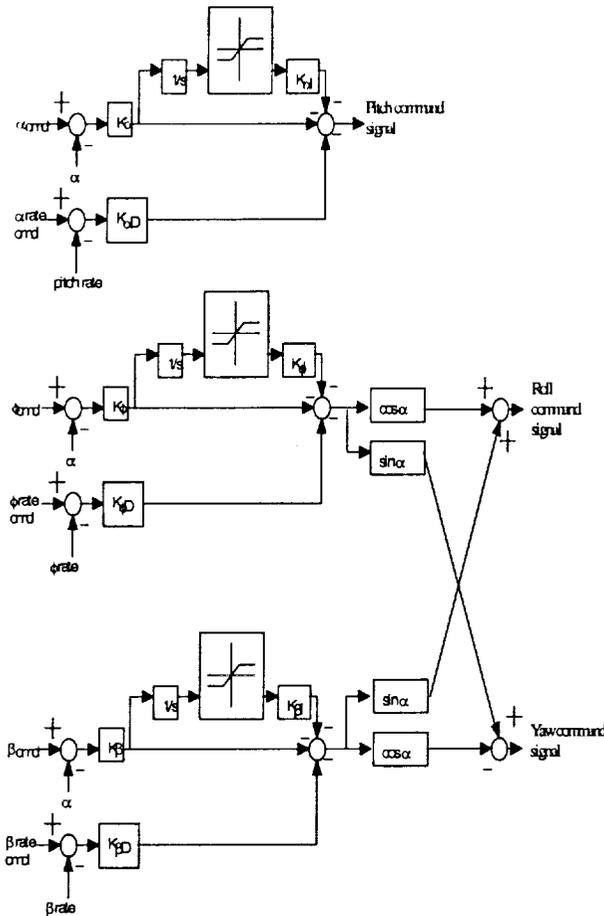
Figure 13: Transition and Entry Control System Simplified

Dispersions that have been run have indicated the system is insensitive to many mechanical tolerances. Key dispersions appear to be aerodynamics (which have relatively high uncertainties) and atmospheres, which can lead to both recoverable events (such as rollovers) and unrecoverable events (usually manifested as loss of β control). Increasing tolerance to these problems is a primary concern as the design reaches its final stage, but the structure is expected to permit development of solutions within the limits of the available control authority.

References:

[1] Reusable Launch Vehicle Single Stage To Orbit WB001 Flight Mechanics Data Book, November 29, 1994

[2] Reusable Launch Vehicle Single Stage To Orbit VL001 Flight Mechanics Data Book, April 1995

[3] MARSYAS User's Manual Revision 8, March 22, 1996

[4] Maveric User's Guide, August 19, 1997

[5] Optimal Control Allocation for the X-33, ED11(13-98-125), Mark E. Jackson, May 21, 1998

[6] Control System Model of an Airframe Flex Model With Application to X-33, Mike Hannan, May 15, 1998

[7] Flight Dynamics and Stability and Control Characteristics of the X-33 Vehicle, AIAA 98-4410, H. P. Lee, M. Chang and M. K. Kaiser, Aug. 10, 1998

[8] Deterministic Reconfigurable Control Design for the X-33 Vehicle, AIAA 98-4413, Elaine A. Wagner, John J. Burken, Aug. 10, 1998

[9] "Sliding Mode Control of the X33 Vehicle in Launch and Re-entry Modes," Yuri Shtessel, James McDuffie, Mark Jackson, Charles Hall, Don Krupp, Michael Gallaher, and N. Douglas Hendrix, AIAA98-4414, Proceedings of AIAA Guidance,Navigation, and Control Conference, Boston, MA, August 10-12, 1998

[10] The Dynamics of Liquids in Moving Containers With Applications to Space Vehicle Technology, Abramson, Ed., NASA SP-106, 1966

[11] The NASA/MSFC Global Reference Atmosphere Model - 1995 Version (GRAM - 95), NASA TM 4715, C. G. Justus, W. R. Jeffries, S. P. Yung, and D. L. Johnson, Aug. 1995